What the paper contributes to knowledge?

(1) Numerical analyses of sensitive clay landslides were conducted in 2D in the literature. There is, however, evidence that 2D and 3D yield significantly different results. Therefore, we develop a 3D model to analyze the progressive failure of sensitive clays and validate it with Gjerdrum landslide.

(2) We can quantify the influence of several factors in retrogression distance, including the stress-strain curve of the quick clays (parameterized by a softening rate and a remoulded shear strength) and the terrain and morphology of the quick clay layers.

What evidence the paper created to support the contribution claims?

The model is validated based on observations of Gjerdrum landslides, and back analysis show that there is good agreement between the numerical prediction and in-field observations.

What is particular novel about the insights generated in the research?

A unique feature of this model is that it combines: the reconstruction of a 3D terrain and complicated sensitive clays layers; capability to assign soil properties based on CPTU data; and the calculation of retrogressive distances and the onset of failure in a single, unified manner utilizing large deformation analysis.

Why the contributions matter? (What problems are addressed / What opportunities are created)

The model can be used to investigate the dynamic process of sensitive clays in 3D. As an alternative to empirical methods, it can also be used to predict the retrogressive distances.

What the limitations of the research are?

Limitations of the model are (1) the 3D numerical model is restricted to total stress analysis at a slope scale; (2) numerical predictions require accurate detection of sensitive clay layers and soil properties; (3) Computations are expensive, requiring high-performance computing.

What next steps are suggested?

To capture more realistic failure mechanisms of sensitive clay landslides, effective stress analysis could be an appropriate next step.

3D large deformation modeling of the 2020 Gjerdrum quick clay landslide

Quoc-Anh Tran[1], Agnete Rogstad[1], Ivan Depina[1], Fabricio Fernández[2], Gebray Habtu Alene[1], Gustav Grimstad[1], Steinar Nordal[1]

[1] Department of Civil and Environmental Engineering, Norwegian University of Science and Technology, Norway.

[2] Department of Civil and Environmental Engineering, Pontifical Catholic University of Rio de Janeiro, Brazil.

ABSTRACT

A quick clay slide in Gjerdrum, Norway, occurred at 4 a.m. on 30th December 2020 killing 10 people and destroying houses, roads, and other infrastructures. Approximately 1.35 million cubic meters of clay were released, a large volume liquefied, and debris was transported almost two kilometers downstream. An investigation following the slide determined that the slide was initialized in a 30-meter-high slope after 2-to-2,5-meter vertical erosion in a small creek running along the toe of the slope. After the initiation, the slide developed retrogressively in the order of 500 meters backward and sideways over a period of about 2 minutes. A conventional geotechnical slope stability analysis explains the initial slide. However, more advanced numerical tools are needed to simulate the retrogressive mechanism and the debris flow. The aim of the paper is to demonstrate a 3D Material Point Method model to capture some of the mechanisms involved from initiation until the debris comes to rest, and how this method can be used to reproduce and study the processes involved in large deformation landslides.

KEYWORKS: quick clay, sensitive clay landslides, Material Point Method, large deformation modeling

1 Introduction

Scandinavia and Canada are both at risk of large-scale, sensitive clay landslides. For example, Norway has experienced large, quick clay landslides larger than 50.000m^3 approximately once per year since 1970 (J.S. L'Heureux, 2018). In December 2020, ten people lost their lives in a fatal sensitive clay landslide in Gjerdrum, Norway, and houses and other infrastructure have been destroyed. Due to significant softening after reaching peak strength, most sensitive clay landslides are progressive or retrogressive. It is essential to model the initiation and mobility of sensitive clay landslides to improve future sensitive clay landslide risk management.

Figure 1 Gjerdrum landslide (photo from NVE)

Finite element or limit equilibrium methods can be used to determine the probability of the failure (Locat et al., 2013; Locat et al., 2011), but they cannot capture the mobility of the landslide. By incorporating balance equations along with the depth (refer as depth averaged model), it allows to study the mobility of the sensitive clay landslides (Liu et al., 2021). Due to the fluid dynamic nature, the depth average models cannot simulate the nature of the retrogression. Furthermore, the depth averaged models require to determine how much soil is released in advance which complicates the prediction of the sensitive clay landslide.

For this reason, particle-based methods have become an increasingly popular choice as numerical tools to analyze both the initiation and mobility of the sensitive clay landslides. Few

examples are the coupled Lagrangian-Eulerian method (Dey et al., 2015), the Material Point Method (Tran & Solowski, 2019) , and the Particle Finite Element Method (Zhang et al., 2020). Despite this, all these studies were conducted under plane strain conditions without considering three-dimensional effects. However, the slope stability analyses for two-dimensional and three-dimensional slopes can present significantly different results for natural slopes that have layered soils and complex topography (Alison McQuillan, 2021).

The paper aims to use the Material Point Method to perform a 3D analysis of the Gjerdrum quick clay landslide as a case study. To understand the advantages and limitations of the proposed model, the simulation is compared to observations from the Gjerdrum landslide. A 3D MPM model allows us to study (1) the failure initiation associated with strain localization and (2) the mobility of the liquefied soil such as the size, direction, and distance of progressive failure.

1. Problem definition

A quick clay landslide has three stages: a triggering stage, the onset of failure and a post-failure stage. In the first stage, either natural factors (e.g., erosion) or human activity can trigger the failure. After the onset of failure, the progressive failure occurs involving a rapid movement of liquified soils. In the Gjerdrum landslide, the erosion is speculated to be the major cause to trigger the slide (Ryan et al., 2021). It was demonstrated from 2007 to 2020 with around two meters of soil being eroded by the creek (Figure 3). The Gjerdrum landslide was classified as a quick clay flow landslide under the Varnes' classification of landslides (Hungr et al., 2014). This failure mechanism is typical in Norway. The Gjerdrum landslide was reported to be released retrogressively in nine stages (Figure 2). Several factors contributed to this conclusion, including the photos, the videos, the geotechnical and hydraulic investigations, and the witness testimony. Based on soil investigations, this study aims to replicate the Gjerdrum landslides using a 3D model using the Material Point Method.

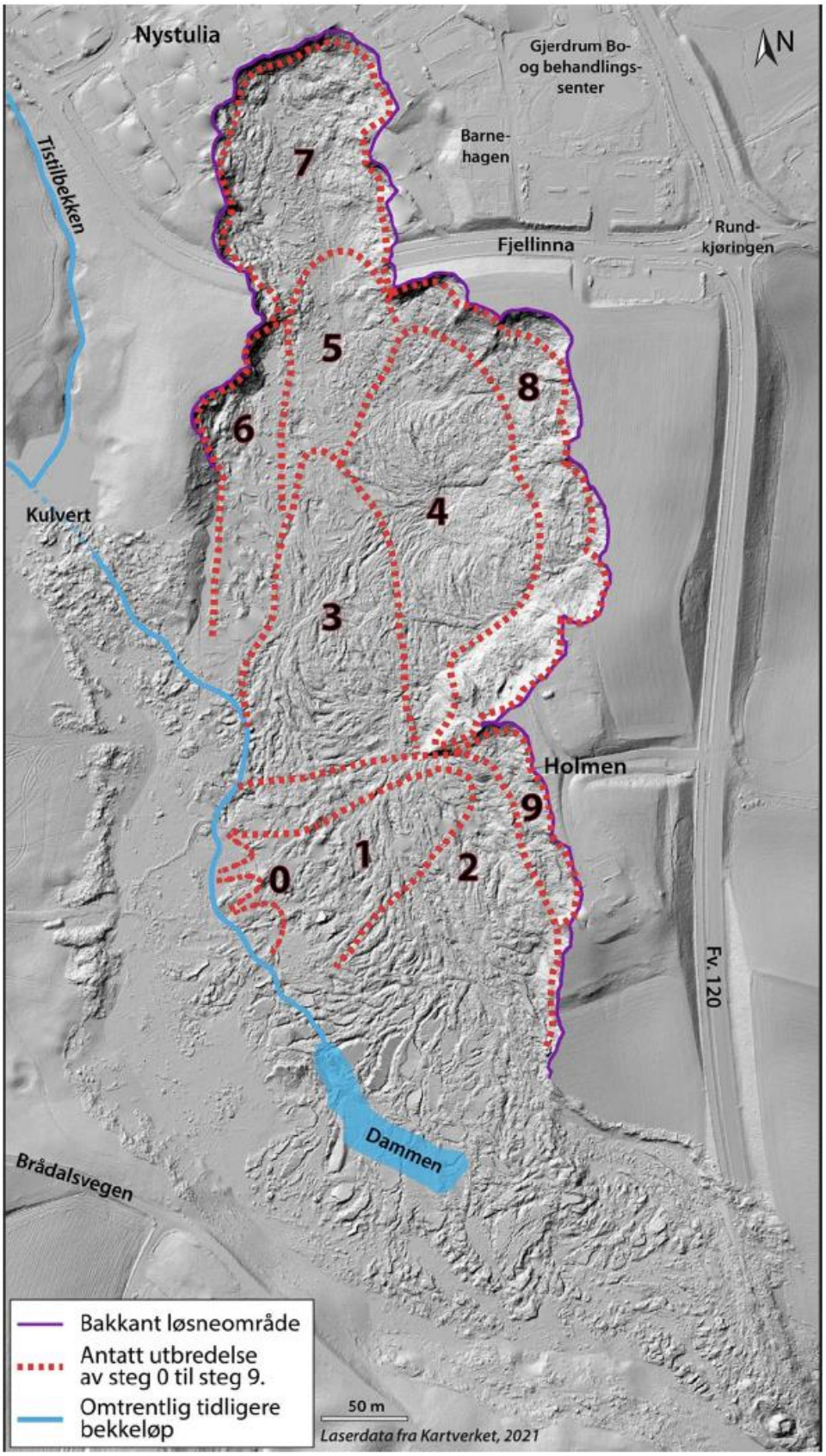

Figure 2 Nine stage of Gjerdrum landslide (Ryan et al., 2021)

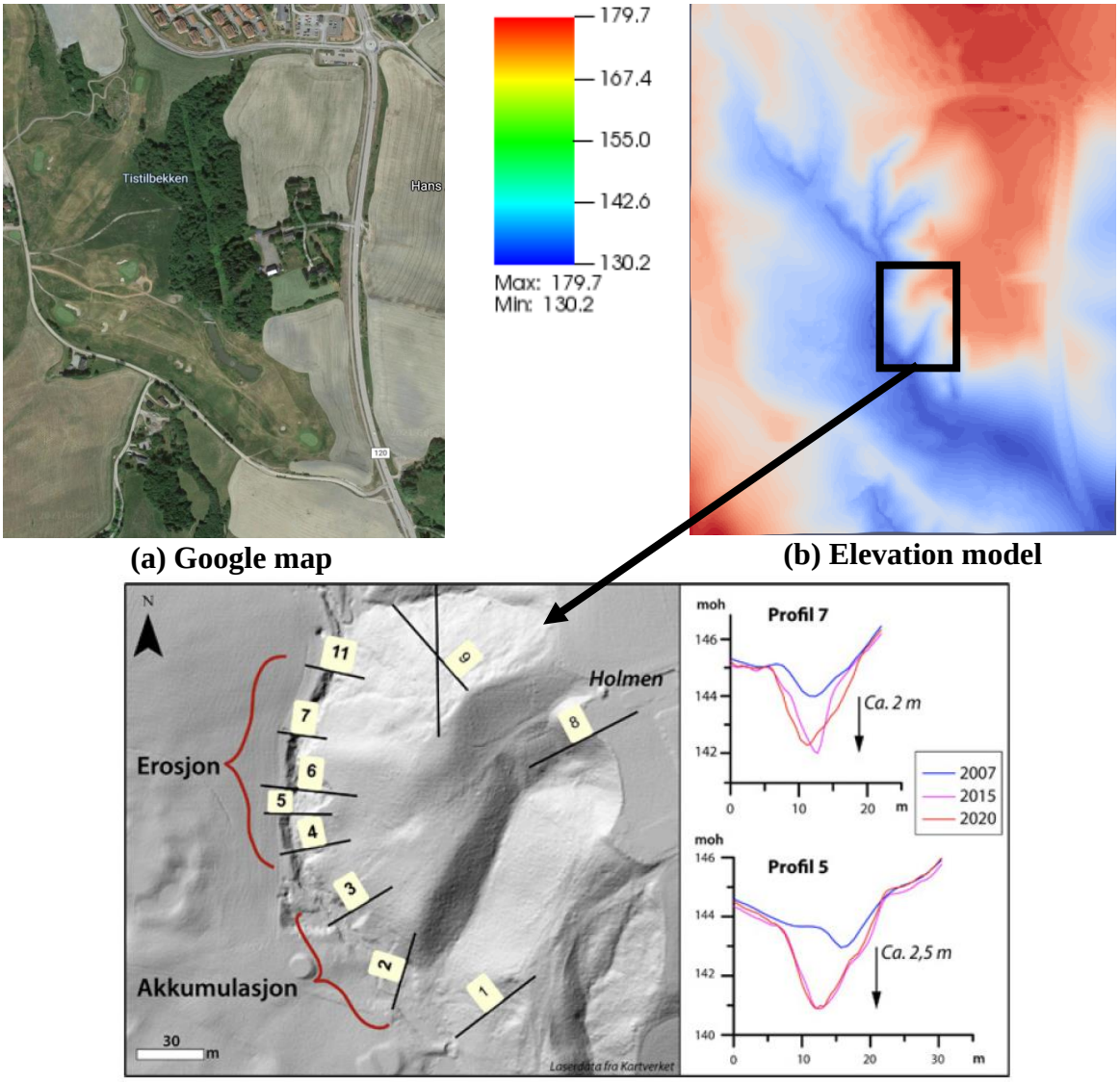

Figure 3 Erosion mechanism (Ryan et al., 2021)

2 Research Methodology

2.1 Hypothesis

- The model does not consider the run-out distance during the landslide mobility but focuses on the analysis of the triggering and retrogressive failure mechanism.
- The model does not account for several important factors related to the failure of slopes. These factors include soil anisotropy, hydraulic conditions, weather conditions, external loads attributable to buildings, or snow accumulations.
- Landslides are primarily caused by erosion. With negligible erosion between 2015 and 2020, the topography of 2015 may be considered to represent the initial ground elevation.

- There are three distinguished layers including bedrock, non-sensitive clay layer and quick clay layer with data obtained from soil investigation. The bedrock is modeled as rigid. The clay layers are modeled using Tresca softening model with a low sensitivity (1-10). The quick clay layers are modeled using Tresca softening model with a high sensitivity (20-100).
- The initial stress is generated using gravity. Because the landslide happened rapidly, the clay layers behave in an undrained state. The undrained parameters are obtained from CPTUs for the entire area. Material properties are retrieved from (Multiconsult, 2021a-a) and (Multiconsult, 2021b).

2.2 Research methodology

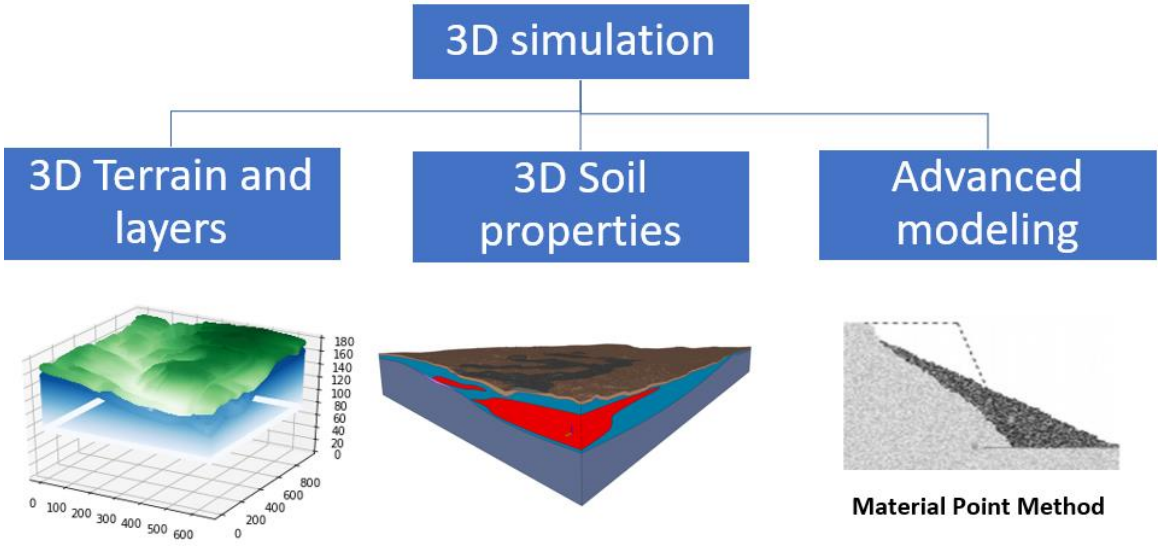

Figure 4 Three-dimensional simulation

There are three components for the implementation of the 3D model (Figure 4) including (1) 3D reconstruction of terrain and soil layers, (2) Assigning 3D soil properties for material points and (3) advanced numerical solvers for large deformation modeling.

(1) The 3D layers of quick clays and bedrock are obtained from the geophysical report.

(2) Soil properties (e.g., undrained shear strength) are interpolated in the entire layer using CPTu data.

(3) Using Material Point Method to simulate the entire process of the Gjerdrum landslide.

3 Three-dimensional terrain and layer model reconstruction

(Digital terrain model analyzed and provided by Gebray, 3D discretization code implemented by Fabricio and analyzed by Agnete, manuscript written by Fabricio)

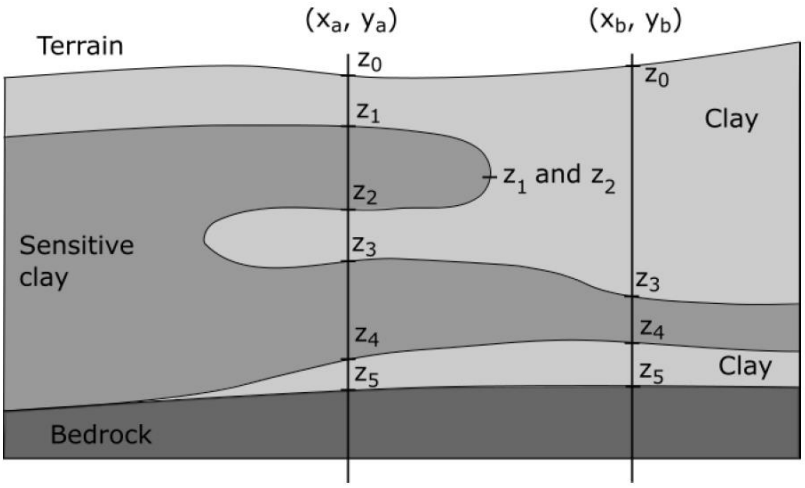

Figure 5 Construct data for layering

Three dimensional models for landslides require spatial discretization of material points to represent the terrain and soil layers. The model in this study combines digital elevation data with 3D MPM discretization (Fernandez et al., 2020). In Figure 5, elevation points ($z_{0\text{-}5}$ in Figure 5) are used to determine the elevation of the soil layers. From the bottom up, the numerical model distributes material points based on elevation and discretization. This methodology allowed the creation of a 3D MPM model with an arbitrary and complex distribution of soil layers and terrain within the domain of analysis. We convert the LeapFrog data of the terrain (Figure 6) and the soil layers (bedrock, clay, quick clay in Figure 8) to materials points in 3D (terrain in Figure 7, bedrock in Figure 9 and quick clay in Figure 10). The 3D model in this study has a grid resolution of 1 meter with 8 material points per element, and it results in the distribution of 117.552.926 material points in a structured grid of 45.924.000 elements. There are 89.471.948 material points in the non-sensitive clay and 28.080.978 material points in the quick clay.

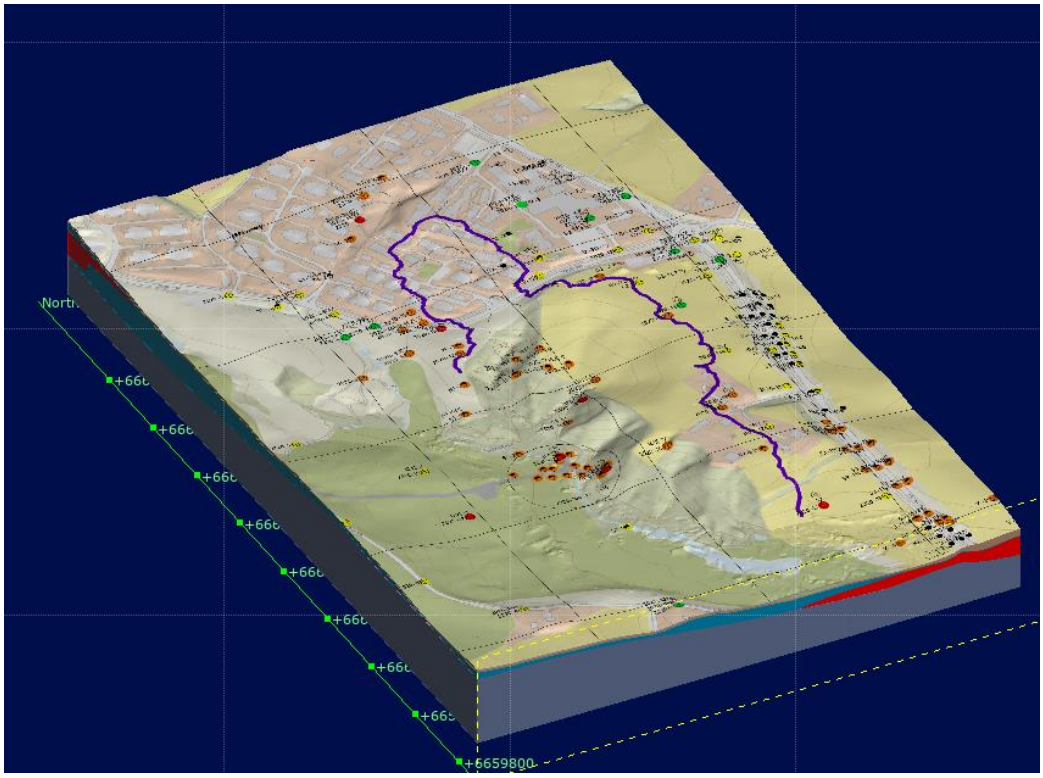

Figure 6 Terrain model in LeapFrog (Multiconsult, 2021a-b)

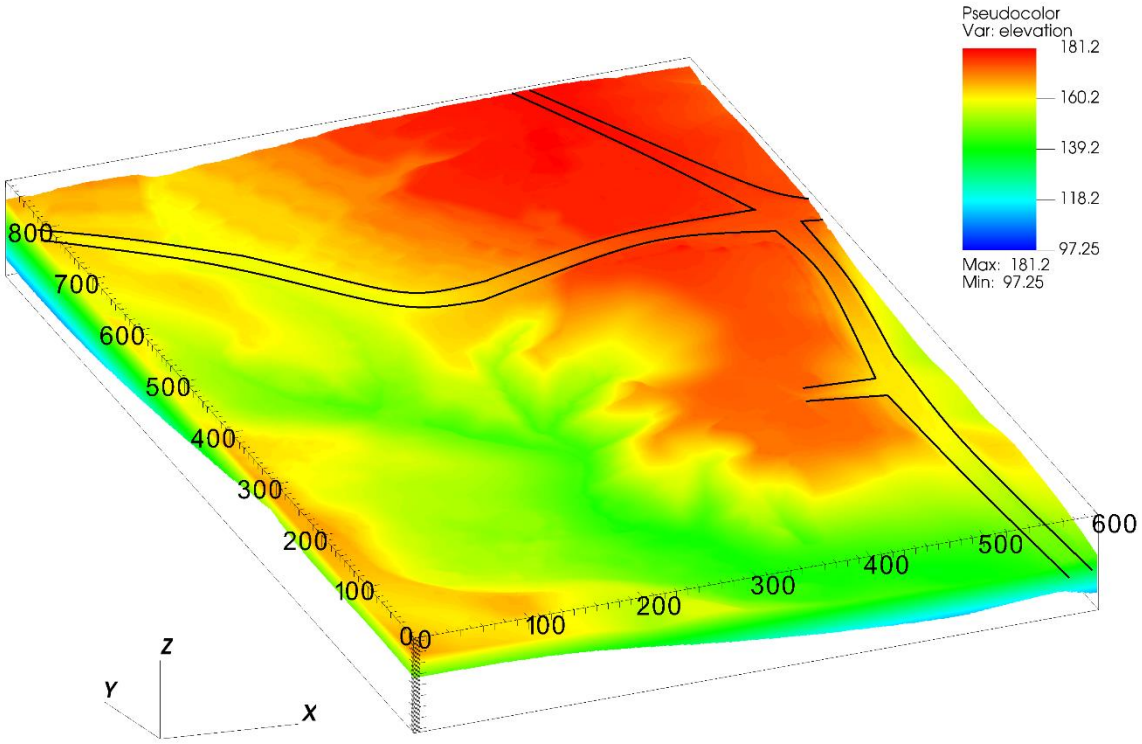

Figure 7 Terrain elevation in numerical model

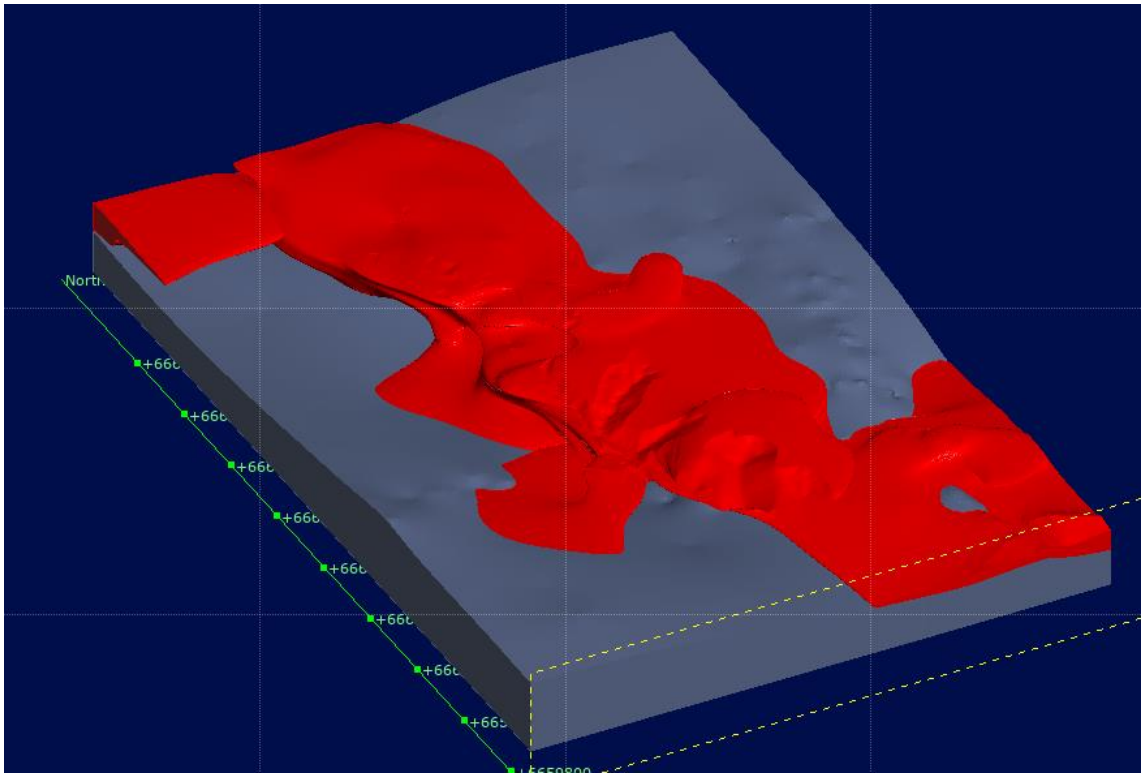

Figure 8 Bedrock and quick clay (red) model in LeapFrog (Multiconsult, 2021a-b)

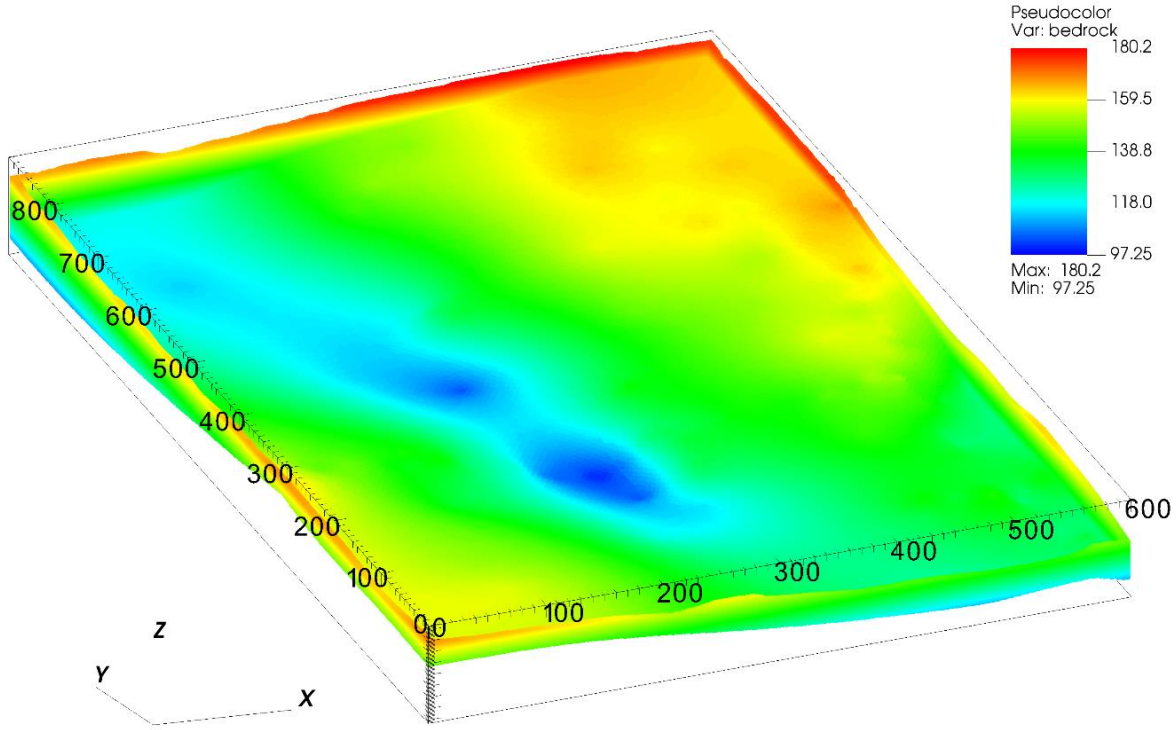

Figure 9 Bedrock elevation in numerical model

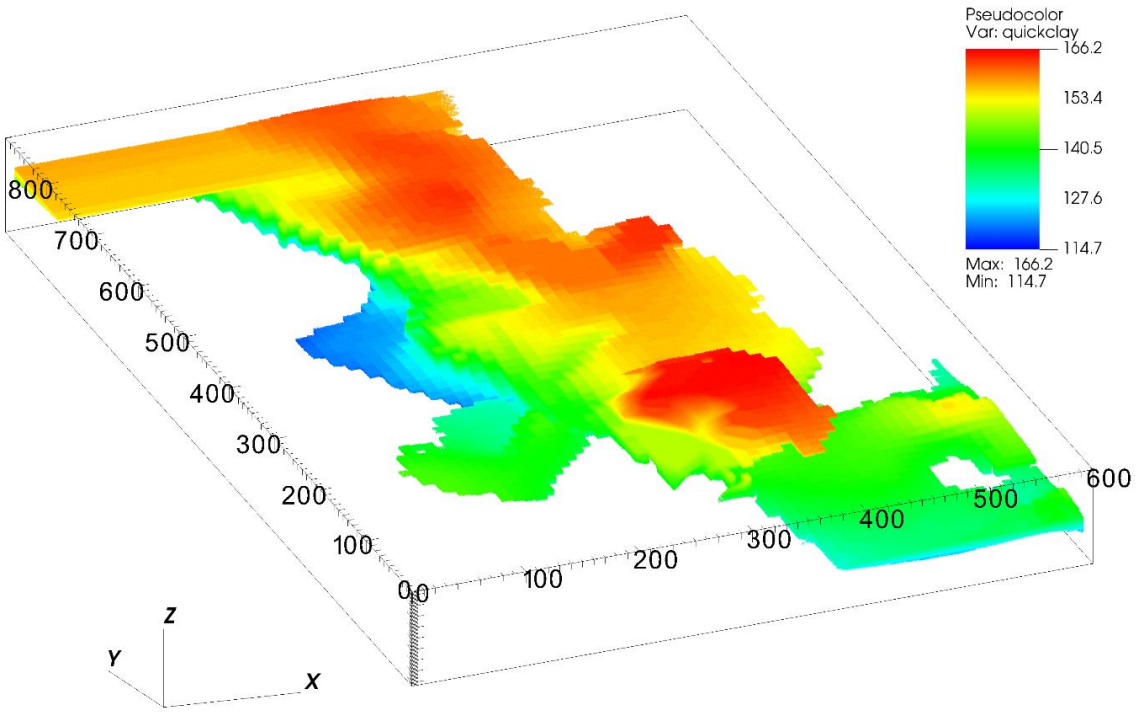

Figure 10 Quick clay elevation in numerical model

4 Assigning 3D soil properties for material points from CPTUs

(Code implemented by Ivan and analyzed by Agnete, manuscript written by Ivan)

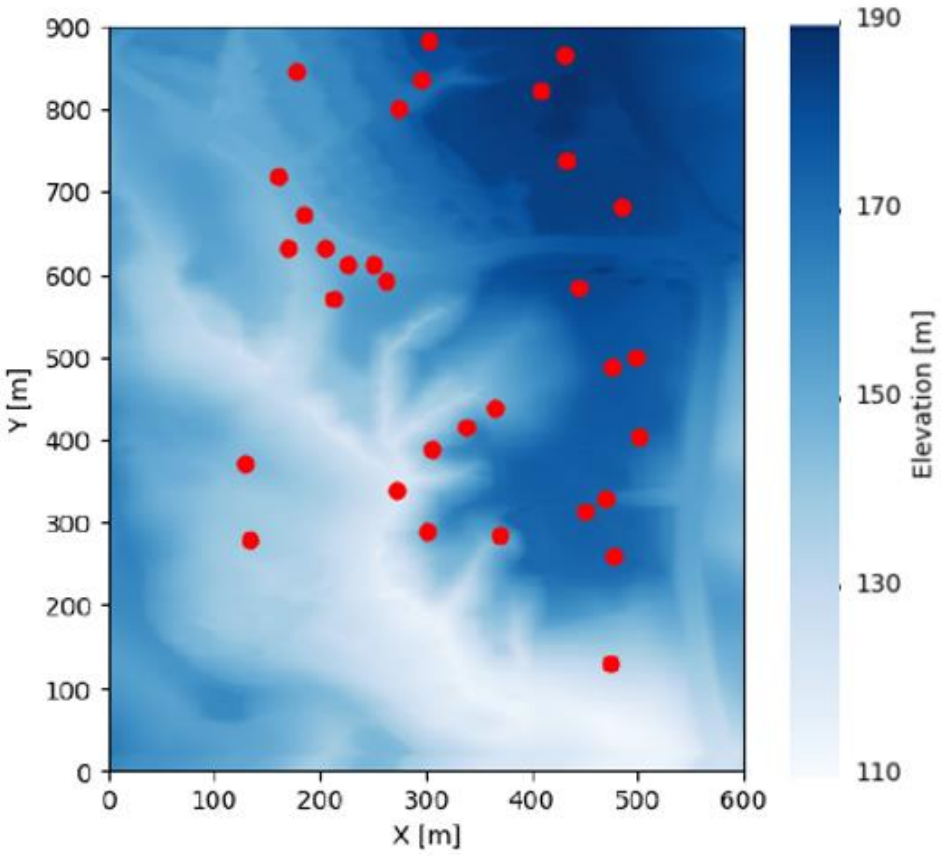

Figure 11 Location of CPTU boreholes

Shear strength values are interpolated across the model domain from 33 interpreted boreholes at the site. The shear strength values in the boreholes are interpreted from available CPTu profiles and laboratory tests (Multiconsult, 2021a-a) and reduced to linear profiles along the depth for improved interpretability. Prior to implementing interpolation, each borehole was discretized into 200 points along the vertical axis. The values of the undrained shear strength were interpolated at these points along the boreholes.

The interpolation of undrained shear strength values from the borehole locations to the rest of the domain was conducted with a Radial Basis Function (RBF) approximation (Rippa, 1999; Virtanen et al., 2020). Let $f(\boldsymbol{d}); \boldsymbol{d} = [x, y, z]^T$ be a real-valued function in the three spatial dimensions that we wish to approximate with RBF. An RBF approximation to $f(\boldsymbol{d})$ is a function s that takes the form (Rippa, 1999):

$$s(\boldsymbol{d}) = \sum_{i=1}^{n} a_i \, \varphi(\|\boldsymbol{d} - \boldsymbol{d}_i\|) \tag{1}$$

where φ is a fixed real-valued radial basis function and $\|\cdot\|$ denotes the Euclidean norm. The points $\boldsymbol{d}_i; i = 1, \dots, n$ are called the centers of the RBF approximation (Rippa, 1999). RBF approximation was selected due to its very simple structure and efficient performance on unstructured interpolation on large numbers of points. Some of the commonly used radial basis functions include gaussian, cubic, linear, inverse, and multiquadric (Rippa, 1999; Virtanen et al., 2020). Radial basis functions commonly include a tuning parameter that needs to be adjusted as it can significantly affect the performance of the approximation. Given n locations, $\boldsymbol{d}_i; i = 1, \dots, n$, and a vector of observations $\boldsymbol{f} = [f_1, \dots, f_n]^T$, where $f_i = f(\boldsymbol{d}_i)$, we aim to find a function $s(\boldsymbol{d})$ of the form in Eq. 1 that interpolates the observations such that (Rippa, 1999):

$$s(\boldsymbol{d}_i) = f_i; i = 1, \dots, n \tag{2}$$

Solving the interpolation in Eq. 2 is equivalent to solving a system of linear equations [1]:

$$\boldsymbol{A}\boldsymbol{a} = \boldsymbol{f} \tag{3}$$

for the coefficient vector $\boldsymbol{a} = [a_1, \dots, a_n]^T$, where $\boldsymbol{A} = A_{ij} = \varphi(\|\boldsymbol{d}_i - \boldsymbol{d}_j\|)$.

The linear radial basis function was used for the interpolation of undrained shear strength values after testing a wide range of radial basis interpolation functions. Selection is primarily based on making sure that shear strength profiles along the depth are realistic and that the computation is efficient. Shear strength profiles are typically characterized by an increase in undrained shear strength with depth and approximately constant values of undrained strength in the dry crust layer. We were not able to replicate these trends using more advanced radial basis functions. In addition, the linear basis function does not require tuning parameters (Virtanen et al., 2020). An RBF interpolation of the undrained shear strength values was implemented using the Python SciPy library (Virtanen et al., 2020).

Using this interpolation technique, we can determine the undrained shear strength of the entire layers, as shown in Figure 12 for the ground surface and Figure 13 for the quick clay layer. The undrained shear strength is correlated with the elevation such that the deeper the soil layer, the higher the undrained shear strength. That is consistent with the CPTUs data in which the undrained shear strength increases linearly with depth in the normally consolidated clay.

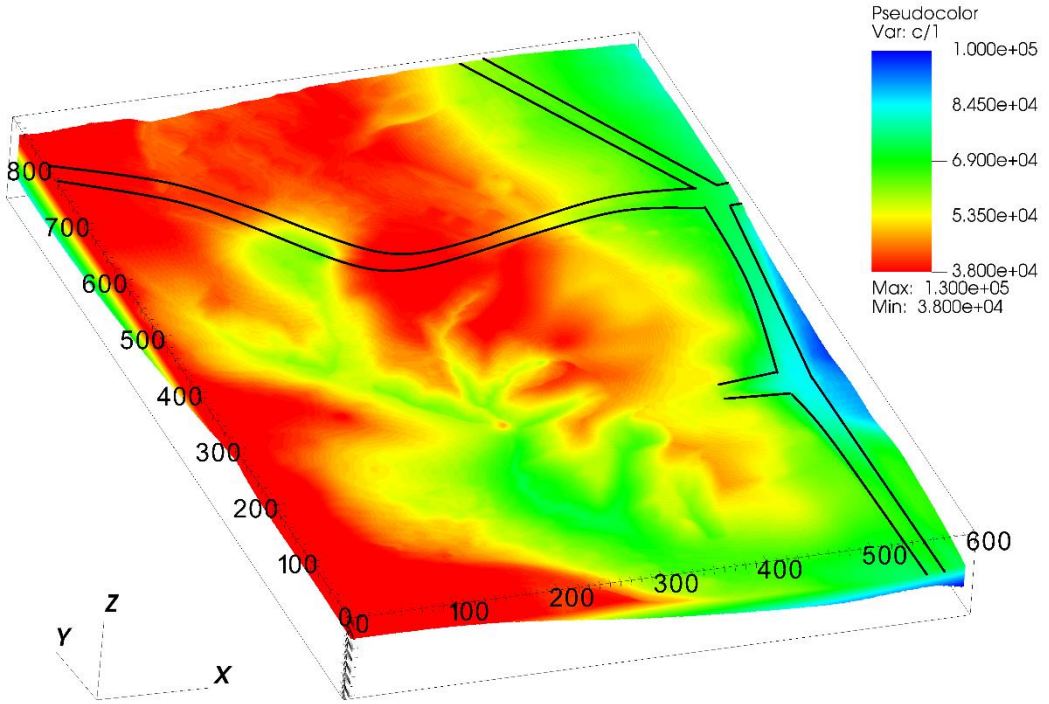

Figure 12 The undrained shear strength at the ground surface

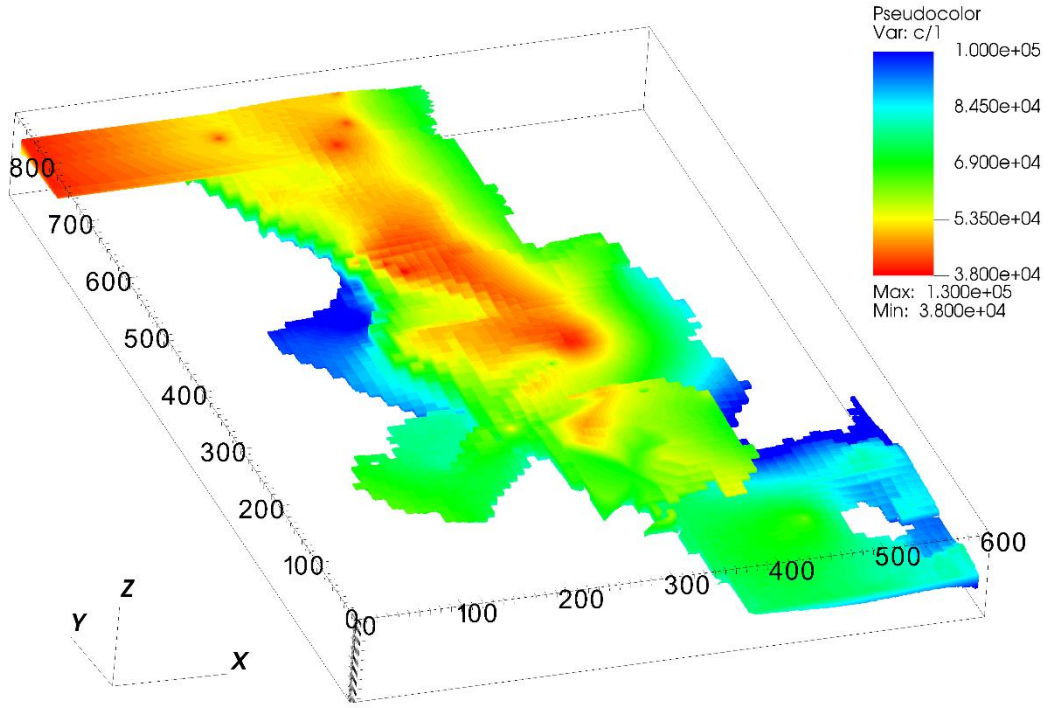

Figure 13 The undrained shear strength of the quick clay layer

5 Numerical model

5.1 Generalized Interpolation Material Point Method

Material point method Based on continuum mechanics; the Material Point Method (MPM) is well suited for the solution of dynamic large deformation problems. Comparing the MPM to the Finite Element Method where the integration points are fixed in the deformed mesh, the MPM allows the integration points, or more precisely the material points, to move freely in the background mesh (see Figure 14). As a result, large deformations in solid mechanics can be modeled for materials that are history dependent. Several years later, Bardenhagen and Kober (2004) proposed the Generalized Interpolation Material Point Method (GIMP), which significantly improves the robustness and accuracy of the original Material Point Method. The GIMP version of the material point method is exclusively used in this paper, as it is coded in the open-source Uintah computational framework. In order to replicate the numerical simulations in this paper, you can find all the implementations on the open-source platform GitHub.

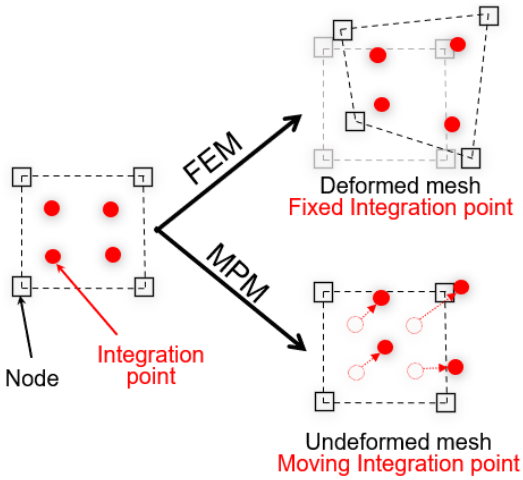

Figure 14 Material Point Method (MPM) vs Finite Element Method (FEM)

5.2 Constitutive model

The paper describes the undrained behavior of clay using an elastoplastic Tresca material model with a non-associated flow rule. There is no plastic volume change during shearing in all simulations in the paper since the dilation angle is assumed to be equal to 0. The shear

strength of sensitive clays decreases with an increase in plastic shear strains. As sensitive clay structure degrades, the shear strength begins to decrease after reaching its peak. Due to this assumption, the undrained shear strength degrades with an increase in shear strain as:

$$s_u(\gamma, S_t) = s_{u,ref}[\frac{1}{S_t} + (1 - \frac{1}{S_t})e^{-3\gamma/\gamma_{95}}] \quad (4)$$

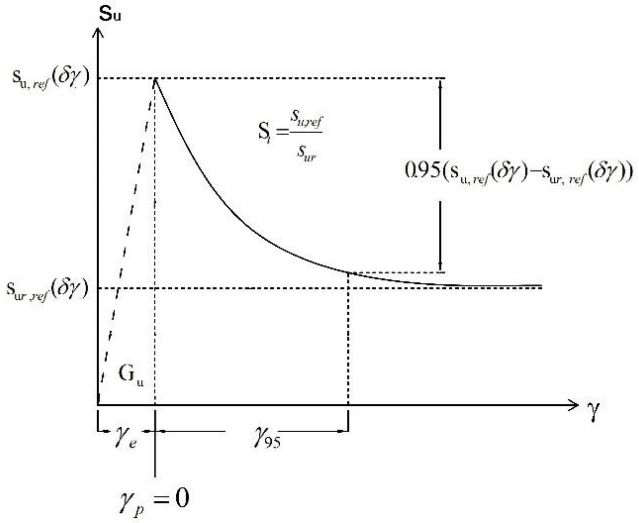

Figure 15 Constitutive model for sensitive clays

where γ is the current accumulated shear strain, γ_{95} is the accumulated shear strains required to obtain 95% reduction of shear strength and the sensitivity S_t is the ratio of undisturbed over remoulded undrained shear strength s_{ur}:

$$S_t = \frac{s_{u,ref}}{s_{ur}} \quad (5)$$

5.3 Geotechnical parameters

Table 1. Parameters in the progressive failure of the quick clays slope

Layer	$s_{u,ref}$ (kPa)	s_{ur} (kPa)	$S_t = \frac{s_{u,ref}}{s_{ur}}$	γ_{95}
Clay	CPTUs data	10	1-10	25%
Quick clay	CPTUs data	0.5	20-100	25%

The average soil density is 19.5 kN/m3 (Multiconsult, 2021a), and is used for all layers. The Young's modulus is set to be 10 MPa with the Poisson's ratio of 0.49. Sensitivity analysis showed that elastic parameters have negligible effects on the numerical results. According to NS8015 (Toril Wiig, 2020), quick clay has a remolded undrained shear strength of less than

0.5 kPa. Therefore, the quick clay layers were calculated using remoulded undrained shear strengths of 0.5 kPa. Meanwhile, CPTUs data indicated that the minimum undrained shear strength in some boreholes is 11 kPa. Therefore, we select a remoulded undrained shear strength of 10kPa for the clay layer. Based on equation (5), the sensitivity of the clay layer is between 1-10 and the sensitivity of the quick clay layer is between 20-100, which corresponds to the results of the fall cone tests in the Gjerdrum landslide. Due to the mesh dependence of this parameter, the parameter γ_{95} (accumulated shear strains required to obtain 95% reduction of shear strength) governing the softening rate is scaled in accordance with the mesh. In several studies (Rogstad, 2021; Tran & Solowski, 2019), γ_{95} was set to be approximately 100% for mesh sizes of 0.25 m. In this study, it corresponds to γ_{95} of approximately 25% for a mesh size of 1 m. The soil parameters for the study are summarized in Table 1.

5.4 Numerical setup and pre-failure initial stress condition

There are two phases to the simulation including (1) Establishing initial stresses using gravity loading; and (2) Using interpreted geotechnical soil properties to study the retrogressive failure process. The first step in the numerical analysis is to simulate the initial stress condition. In order to establish the initial stress condition, all layers are represented by the Mohr-Coulomb non-associated model with drained parameters (cohesion of 20 kPa, friction angle of 30 degrees, and zero dilatancy angle). Using a density of saturated clay (1950 kg/m3), the initial stress in the pre-failure condition was generated by gravity loading. Numerical damping was applied in order to achieve equilibrium more quickly and the numerical damping was removed during the second phase of the simulation. During the initial phase, 5 seconds are required for equilibrium to be established. The same method was also used to analyze the Sainte Monique sensitive clay landslide (Tran & Solowski, 2019). All layers are placed within the rigid bedrock, while all side boundaries operate under Neumann boundary conditions, which facilitates the free movement of debris out of the domain.

6 Numerical results

6.1 Initiation of the first slides

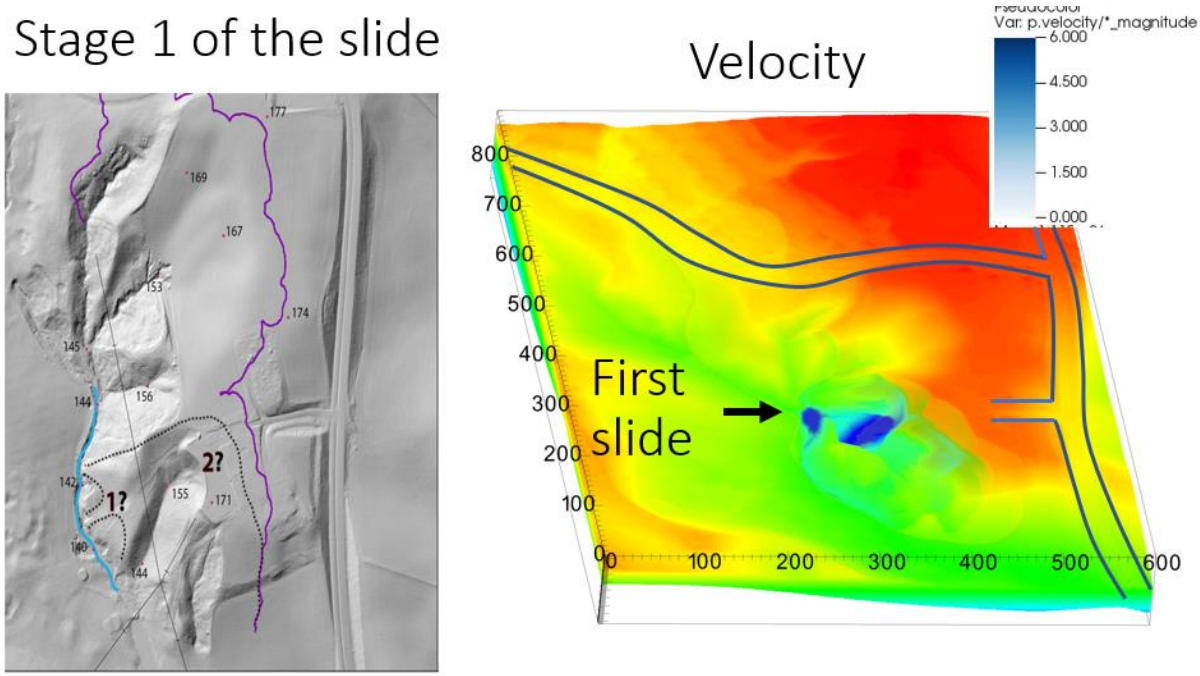

Figure 16 Numerical prediction of the location of the first slides

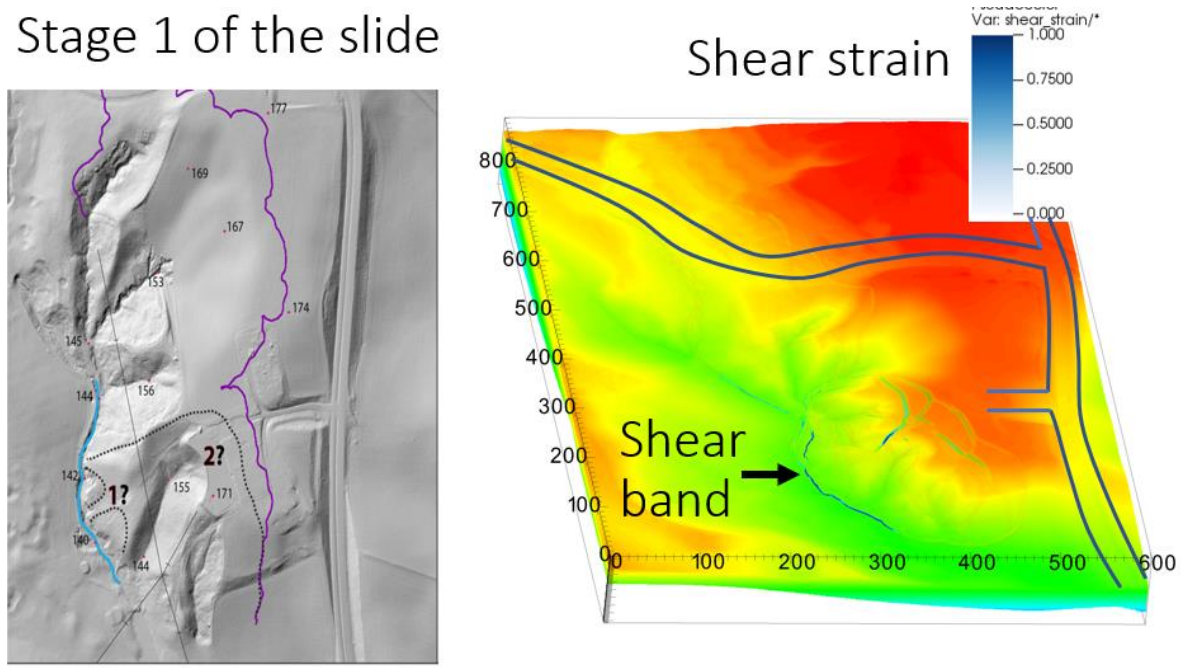

Figure 17 Development of shear band during the initiation of the first slides

The Gjerdrum landslide was initiated by first local instability near Tistilbekken. It is likely that one or more small slides were triggered down the eastern slope of Tistilbekken during the night of 29th to 30th December 2020. In fact, slope stability analysis revealed that these slopes initially

had very low stability (with a safety factor of approximately 1). Due to the instability and the high sensitivity of the quick clays, the numerical model showed that first slides occurred without additional numerical intervention. Here are some numerical observations during the initiation of the slide:

- The numerical model indicated the location of the first slides in a manner similar to that reported in the Gjerdrum report (see Figure 16 where the blue color indicates the speed of the first soil blocks). It is possible to achieve this since the model is capable of reproducing the quick clay layers with a high sensitivity. Indeed, the quick clay layers are quite shallow at the location of the first slides (at 166 m in Figure 10, compared to the terrain's elevation of around 170 m in Figure 7).
- In addition to predicting the movement of the first slides, the numerical model showed a 3D propagation of shear bands or a very thin weak layers along the toe slope near the creek (blue color indicates the magnitude of the shear strain in Figure 17). As shear bands/fractures propagated backward during the retrogressive failure, these shear band were primarily governed by the morphology of the quick clay layers during the retrogressive failure.

6.2 Progressive failure mechanism

This section demonstrates a retrogressive failure in the 3D numerical model and compares it with what was reported on site. The first slides in the Gjerdrum landslides were reported to induce a backward propagating fracture pattern. Following this, landslide masses flowed to the southwest (stages 0, 1, 2 in Figure 2). The quick clay on the slope west of Holmen was stirred and flowed away, leaving a steep, unstable slope to the north. Therefore, retrogressive failure occurred with quick clay debris flowing mainly towards the south. In Stage 7, the landslide event hit Nystulia, and the landslide masses destroyed buildings along the western side of the landslide area.

Using the numerical model, the entire retrogressive failure can be captured (see Figure 18 for snapshots taken at 20 seconds, 50 seconds, 60 seconds, and 120 seconds; the blue color indicates the magnitude of the shear strains). Approximately 20 seconds after the first slide, the soil remoulded and flowed away to the southwest (the black arrow in Figure 19 indicates the direction of the landslide mass movement). The shear bands/fractures propagated to the north at 50 seconds (see the black dashed line in Figure 19). Retrogressive failure occurred immediately following the propagation of the shear band at 60 seconds, with remoulded quick clay flowing mainly to the south. On the east side of the landslide, the soil mass collapsed after 60 seconds due to the remoulded clay continuing to liquefy. Further soil movement to the west was induced as a result of this, which was overestimated in comparison with what was observed on site. At 120 seconds in the simulation, the final deposition can be observed.

In Figure 19, we plotted two cross sections A-A and B-B in order to better understand the simulation process. These cross-sections were chosen because they captured the main directions of flow. The cross section A-A captures the first part of the landslide flowing towards the west, whereas the cross section B-B captures the part of the landslide flowing towards the south. According to the Varnes' classification of landslides (Hungr et al., 2014), the cross section A-A showed the failure mechanism as **clay rotational slides**. This is due to the sliding of the soil mass along a rotational rupture surface with rapid movement of the sensitive clays (see Figure 20). The cross section B-B, however, clearly displayed a **retrogressive flow slide** according to Varnes' classification (Hungr et al., 2014). The failure is characterized by a rapid flow of liquefied sensitive clays with multiple retrogressive clay blocks dislocated and remoulded (see Figure 21).

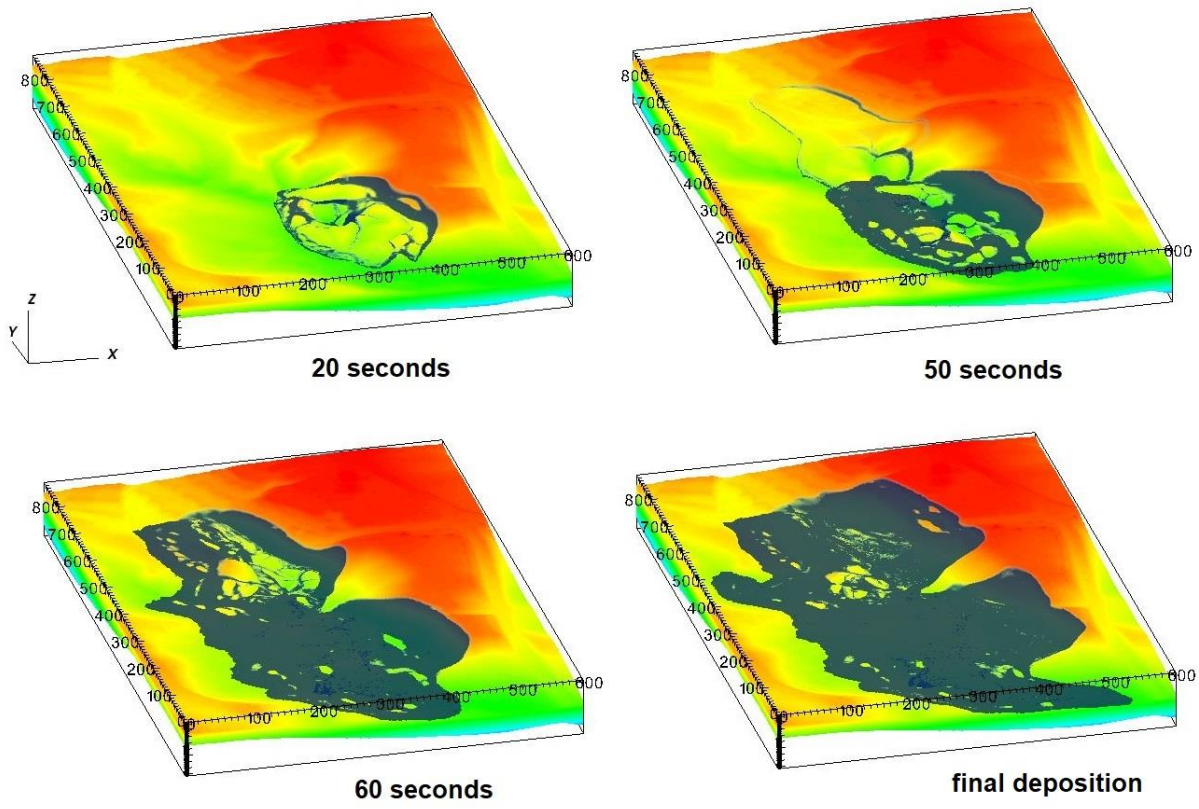

Figure 18 Development of soil movement after the first slides

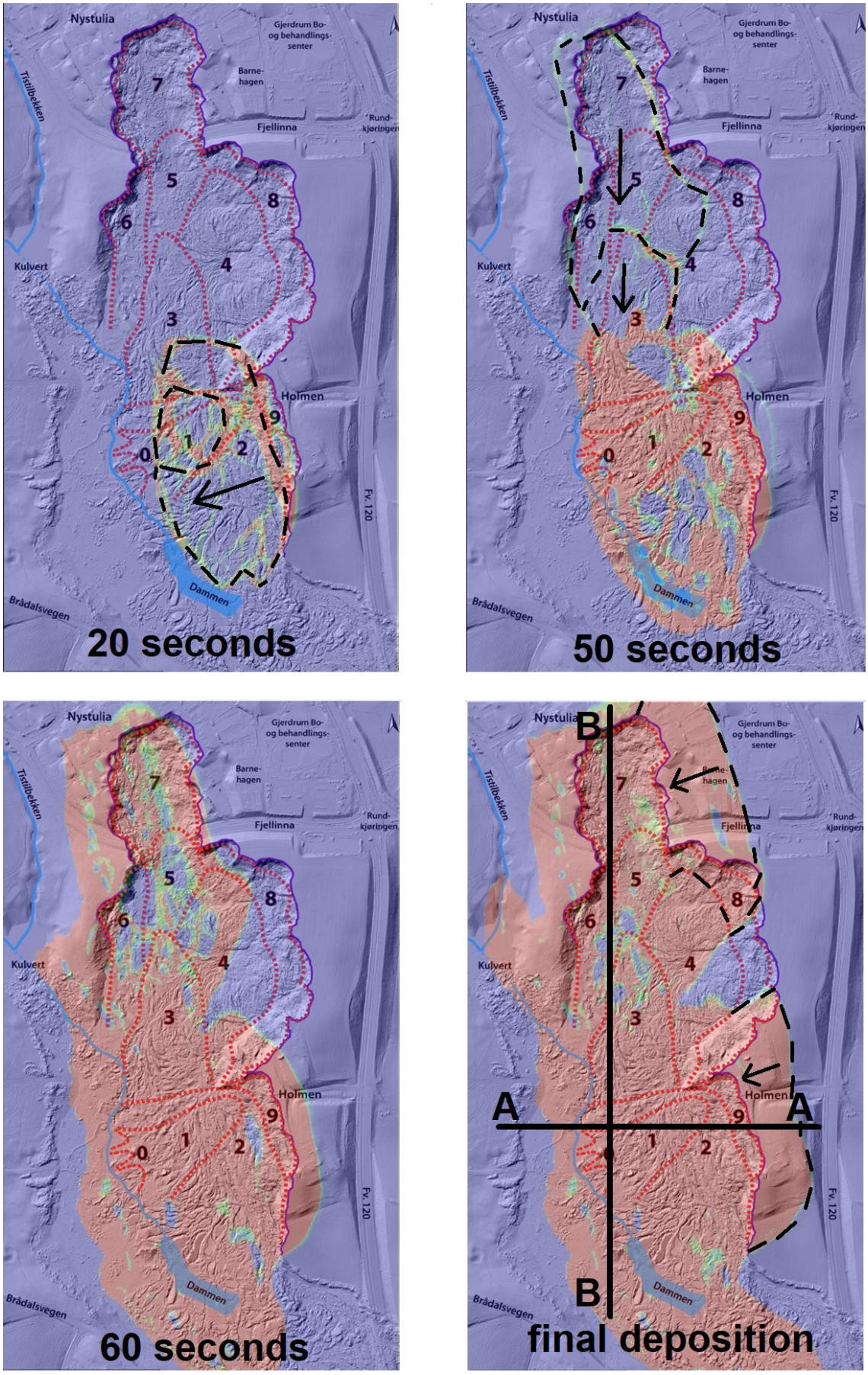

Figure 19 Development of shear band of the first slides

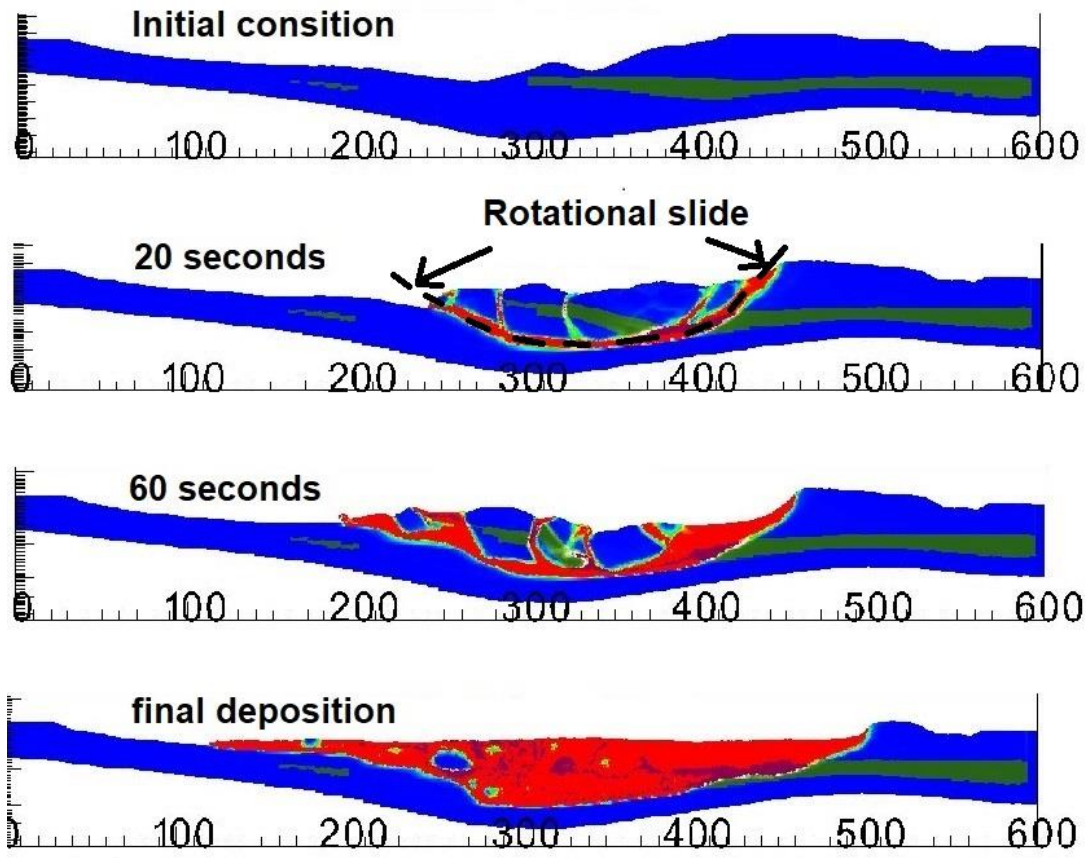

Figure 20 Development of shear bands in cross section A-A

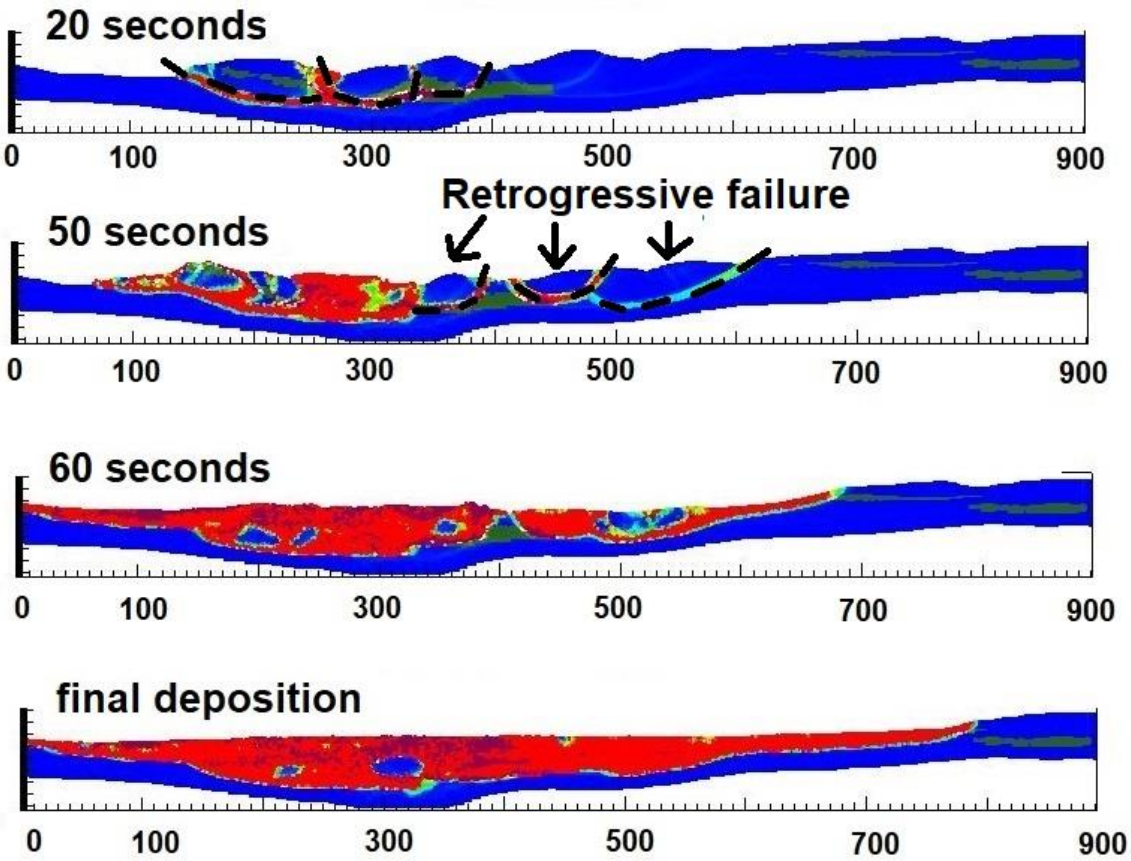

Figure 21 Development of shear bands in cross section B-B

6.3 Influence of stress-strain curve in retrogression distances

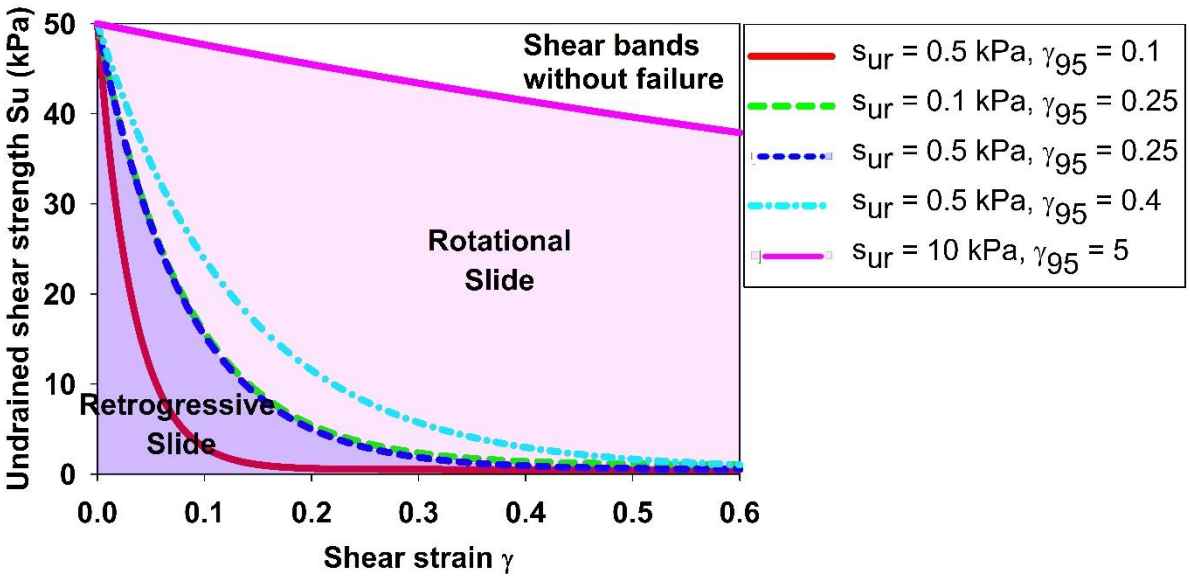

Figure 22 Influence of stress-strain curve in the failure mechanism

In this section, we examine the influence of stress-strain behavior on the failure mechanism of sensitive clay landslides. The stress-strain curve is assumed to satisfy equation (4). Thus, stress-strain behavior is governed by two parameters. The first parameter is the remoulded undrained shear strength of the clay. The second parameter is the accumulated shear strain required to obtain a 95% reduction in shear strength. It is important to note that the former illustrates the sensitivity of clay, while the latter controls how quickly a material will soften. A sensitivity analysis revealed that there are three different mechanisms (see Figure 22) that depend on the softening rate of the material:

(1) The shear bands develop without failure: there is no movement of the soil mass (similar patterns emerge in Figure 17 but with a smaller magnitude of shear strain). The failure mechanism is associated with clay with low sensitivity and low softening rate, with the remoulded undrained shear strength of 10 kPa and γ_{95} equal to 5.

(2) Rotational slides: If the clay has a higher sensitivity and a higher softening rate, rotational slides will occur as the major failure mechanism illustrated in Figure 20.

Therefore, the retrogressive distance was lower than what was observed on site (see Figure 23).

(3) Retrogressive slides: When the clay has an extremely high sensitivity and significant rate of softening, such as the remoulded undrained shear strength of 0.5 kPa and γ_{95} less than 0.25, retrogressive slides are observed with the failure mechanism shown in Figure 21. As a result, the retrogressive distance was higher and closer to what was observed on site (see Figure 24). Reducing either the remoulded undrained shear strength and/or γ_{95} (from the threshold s_{re}=0.5 kPa; γ_{95} = 0.25) had negligible effects on the final retrogressive distances because the landslides almost reached the vicinity of the bedrock layer.

Our study demonstrates the influence of stress-strain behavior on the failure mechanism of sensitive clay landslides. However, this analysis is based on the hypotheses that (a) each layer of soil is homogeneous, and the stress-strain relationship based on equation (4) which was used to average the mechanical behavior of the clay; (b) the stress-strain curve is constructed with the mesh size (1m mesh in this case) in order to prevent strain localization. Other mesh sizes requires scaling adjustment. In the literature, the scaling method has been shown to mitigate mesh dependence in landslide analysis (Tran & Solowski, 2019).

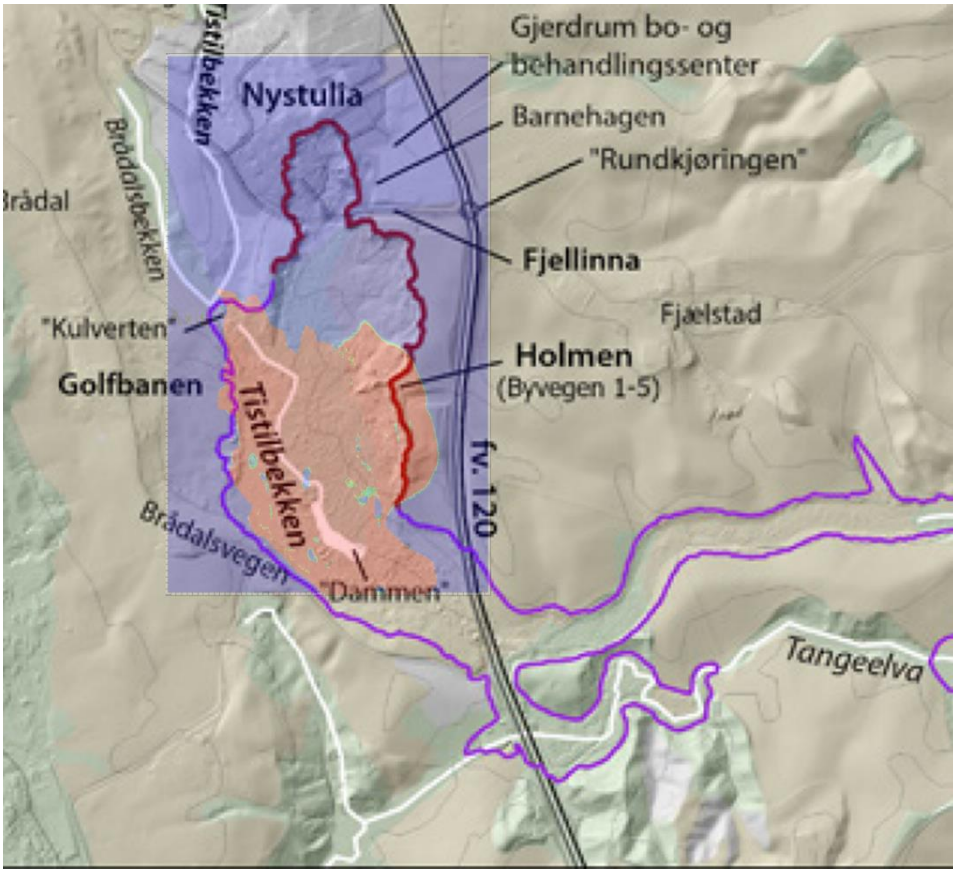

Figure 23 Prediction of retrogression distance in the case of rotational slides

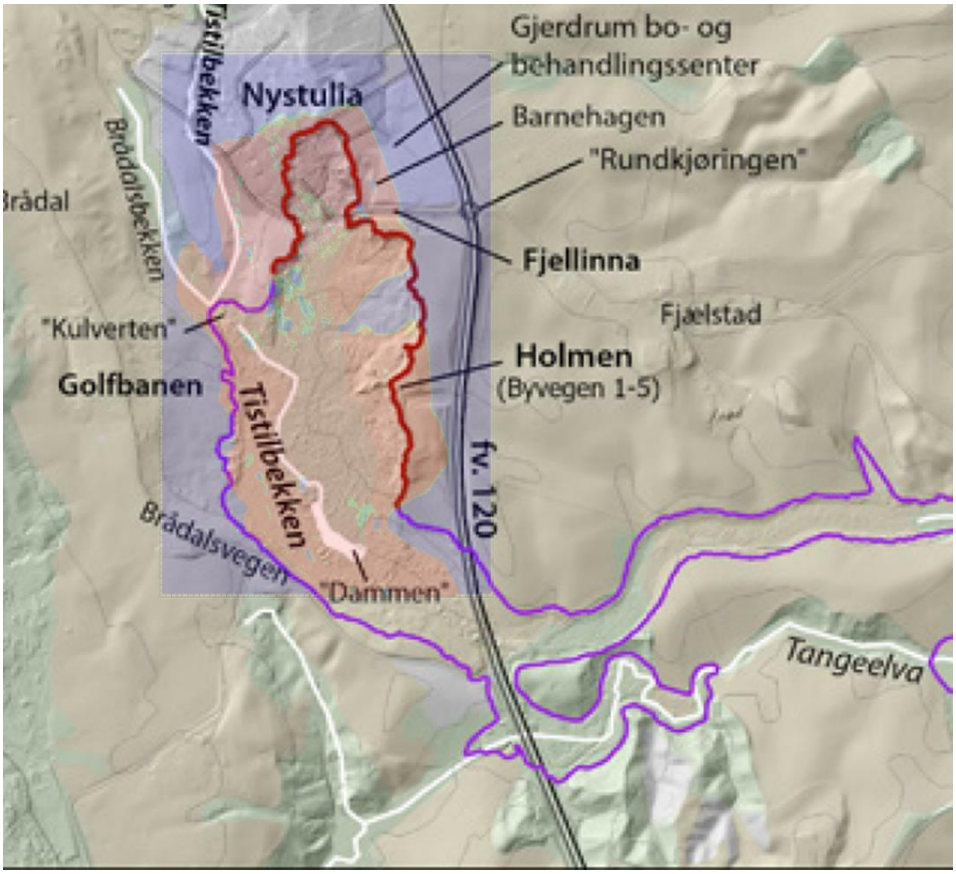

Figure 24 Prediction of retrogression distance in the case of retrogressive slides

7 Empirical methods

(Analyzed by Agnete, manuscript written by Q A)

In Norway, The Norwegian Water Resources and Energy Directorate – NVE published empirical methods to estimate the retrogressive distances in the quick clay landslides based on 40 historic landslides where the retrogressive distance higher than 100 meters. In brief, the empirical method (Toril Wiig, 2020) implies that a retrogressive failure might occur if (1) the remolded shear strength of brittle materials is lower than 1kPa (NS8015) or 0.69 kPa (ISO 17892) and the quick clay layer is deep (the ratio b/D > 40% where b is the depth of the brittle materials and D is the depth of the sliding plane in Figure 25). The susceptible zone to retrogressive failure is estimated above the 1:15 line where the 1:15 line is drawn as a tangent the critical sliding plane and further up the slope (Figure 25). However, the start of the 1:15 line is set to a maximum depth of 0.25H where H is the slope height from where the sliding plane emerges down the slope.

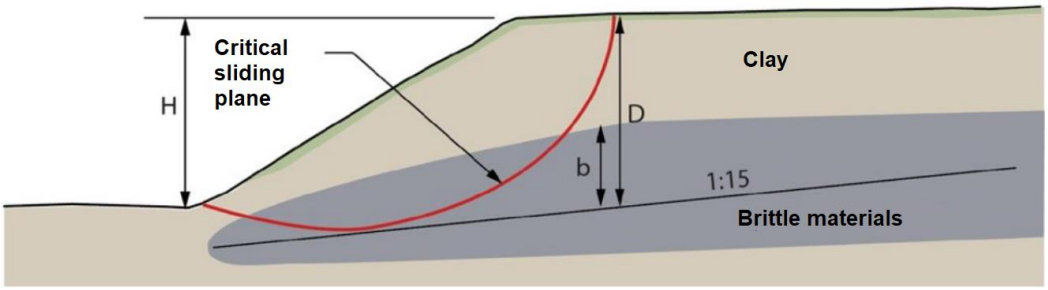

Figure 25 Empirical model from NVE (Toril Wiig, 2020)

As an example of a conservative approach, Rogstad (Rogstad, 2021) estimated the susceptible zone to retrogressive failure in the Gjerdrum landslide using three methods (see Figure 26) without requiring a stability analysis. Assuming that there is only a digital terrain model, method A draws the 1:15 line straight up the slope from the toe to the surface. Method B, on the other hand, assumes that there is a digital terrain model and bedrock morphology, and the 1:15 line changes to 1:3 as it approaches the bedrock surface. Method C, also known as the NGI method (Gregersen, 2010), requires that the morphology of the quick clay layer is known so that the 1:15 line changes to a 1:3 line as it approaches the bedrock or the end of the quick

clay layer. These methods adopt for 2D analysis with simplified soil layers. In 3D, multiple cross sections are determined to perform empirical analysis (see Figure 27). We show that the numerical and empirical methods show a satisfactory agreement in terms of retrogression distances. There is a discrepancy between the numerical simulations and the observation in the blue zone (see Figure 28) because this area has a low elevation with the high undrained shear strength. The implication in Figure 22 is that detecting the quick clay layers are crucial for estimating the retrogressive distances for both numerical and empirical methods. Recent preliminary study on the Gjerdrum landslide (Tran et al., 2022) showed that the 3D model overestimated the retrogressive distance without the detection of the quick clay layers. On the other words, the retrogressive distances could be overestimated if the quick clay layers are unknown.

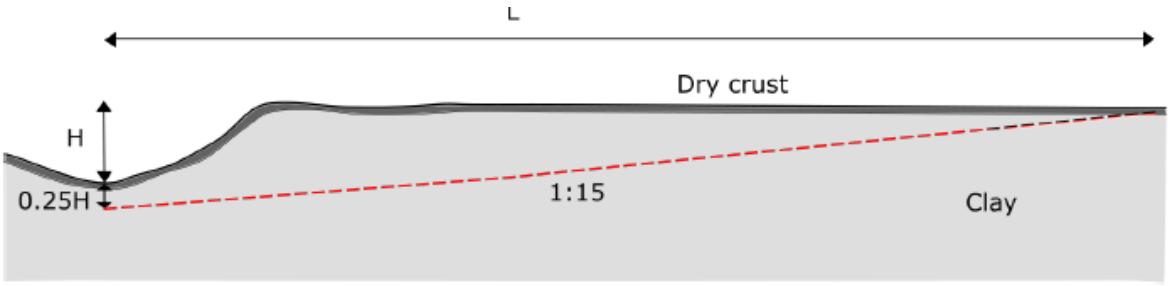

Method A: 1:15 line with no information on bedrock or quick clay layers

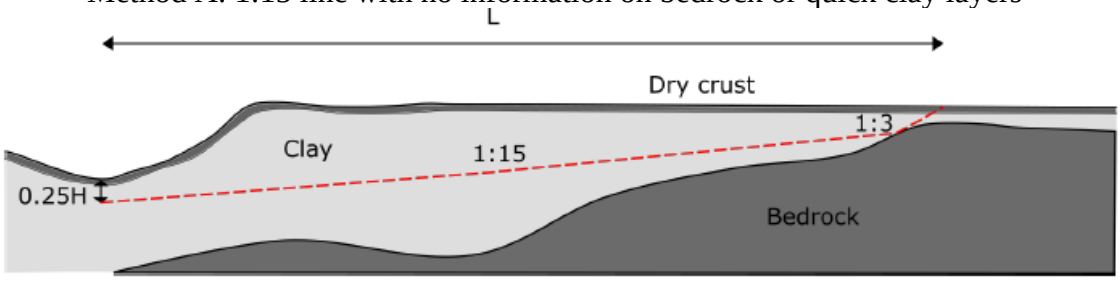

Method B: 1:15 line with information on bedrock only

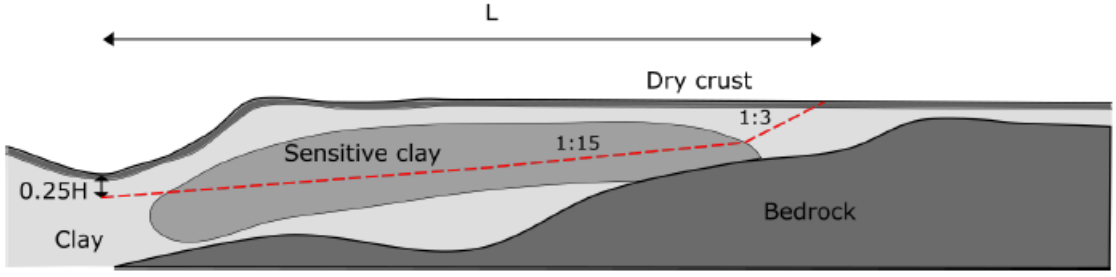

Method C: 1:15 line with information on bedrock or quick clay layers

Figure 26 Different empirical methods (Rogstad, 2021)

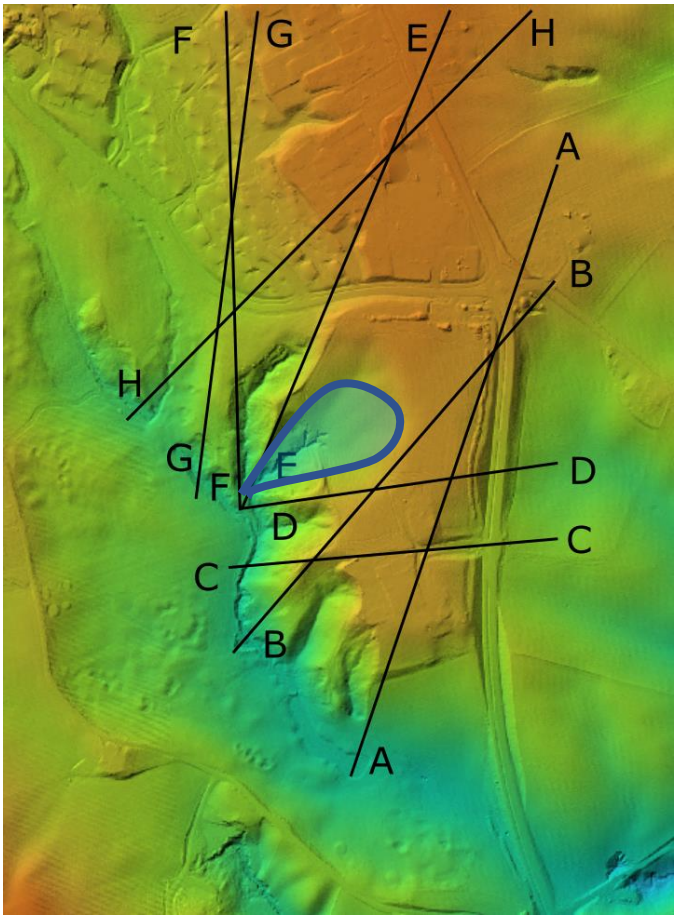

Figure 27 Different cross-section for empirical analysis (Rogstad, 2021)

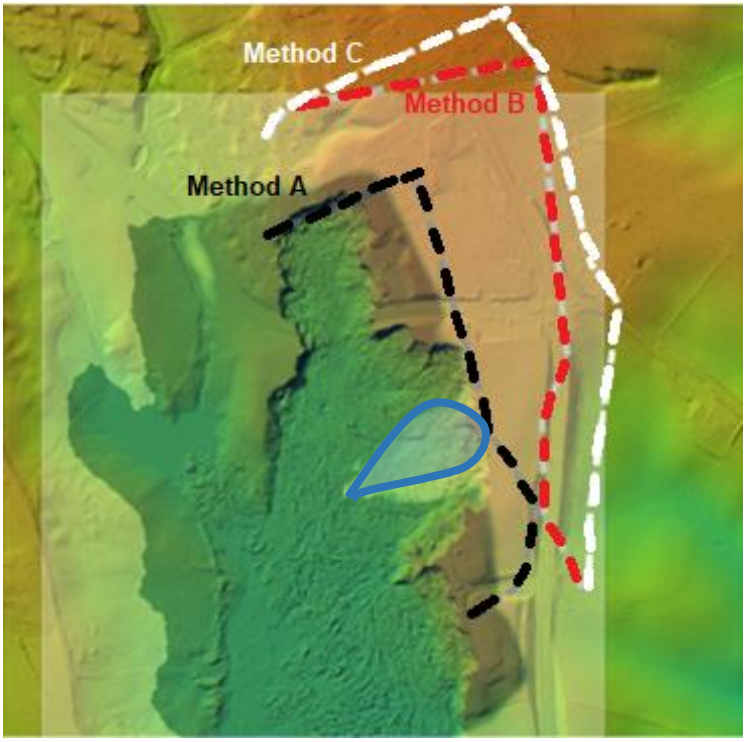

Figure 28 Results of empirical solutions (dash line) and the numerical solutions (black area)

8 Conclusion

In the literature, numerical analyses of sensitive clay landslides are typically conducted using a 2D model. There is, however, evidence that 2D and 3D can yield significantly different results. For this reason, we develop and validate a 3D model that can be used to analyze the progressive failure of sensitive clays. In this study, the model is validated based on observations of Gjerdrum landslides, and there is good agreement between the numerical prediction and in-field observations. A unique feature of this model is that it combines: the reconstruction of a 3D terrain and complicated sensitive clays layers; the assignment of 3D soil properties based on CPTU data; and the calculation of retrogressive distances and the onset of failure in a single, unified manner utilizing large deformation analysis. The model can be used to investigate the dynamic process of sensitive clays in three dimensions. As an alternative to empirical methods, it can also be used to predict retrogressive distances. Limitations of the model are: (1) the 3D numerical model is restricted to total stress analysis at a slope scale; (2) numerical predictions require accurate detection of sensitive clay layers and soil properties (stress-strain) to avoid the overestimation of the retrogressive distances; (3) Computations are expensive, requiring high-performance computing facility. To capture more realistic failure mechanisms of sensitive clay landslides, effective stress analysis could be an appropriate next step.

9 Acknowledgements

The authors gratefully acknowledge Dr. Samson Abate Degago from Norwegian Public Roads Administration for constructive discussion. The research received support from the European Union's Horizon 2020 research and innovation program under the grant agreement 101022007. The computations were performed on High Performance Computing resources provided by UNINETT Sigma2 - the National Infrastructure for High Performance Computing and Data Storage in Norway.

10 Code availability

Instructions for replicating the numerical results in this paper are given at the open-source platform GitHub. Also, the open-source code is shared in this platform for interested users to take up and make use of the results.

11 Reference

Alison McQuillan, N. B., T. Yacoub. (2021). On the comparison of 2D and 3D stability analyses of an anisotropic slope. RIC2021: Rocscience International Conference, Toronto, Canada.

Dey, R., Hawlader, B., Phillips, R., & Soga, K. (2015). Large deformation finite-element modelling of progressive failure leading to spread in sensitive clay slopes. *Geotechnique*, *65*(8), 657-668. https://doi.org/10.1680/geot.14.P.193

Fernandez, F., Vargas, E. D., & Velloso, R. Q. (2020). A 3D discretization procedure for the material point method (MPM). *Computational Particle Mechanics*, *7*(4), 725-733. https://doi.org/10.1007/s40571-019-00303-7

Gregersen, O. (2010). *O. 20091655-00-16-TN Sande, Gunnestad. Utstrekning av eventuelt kvikkleireskred*.

Hungr, O., Leroueil, S., & Picarelli, L. (2014). The Varnes classification of landslide types, an update. *Landslides*, *11*(2), 167-194. https://doi.org/10.1007/s10346-013-0436-y

J.S. L'Heureux, O. A. H., A.P. Paniagua-Lopez, S. Lacasse. (2018). Impact of climate change and human activity on quick clay landslide occurrence in Norway. Second JTC1 Workshops on Triggering and Propagation of Rapid Flow-like Landslides, Hong Kong.

Liu, Z. Q., L'heureux, J. S., Glimsdal, S., & Lacasse, S. (2021). Modelling of mobility of Rissa landslide and following tsunami. *Computers and Geotechnics*, *140*. https://doi.org/ARTN 104388

10.1016/j.compgeo.2021.104388

Locat, A., Jostad, H. P., & Leroueil, S. (2013). Numerical modeling of progressive failure and its implications for spreads in sensitive clays. *Canadian Geotechnical Journal*, *50*(9), 961-978. https://doi.org/10.1139/cgj-2012-0390

Locat, A., Leroueil, S., Bernander, S., Demers, D., Jostad, H. P., & Ouehb, L. (2011). Progressive failures in eastern Canadian and Scandinavian sensitive clays. *Canadian Geotechnical Journal*, *48*(11), 1696-1712. https://doi.org/10.1139/T11-059

Multiconsult. (2021a-a). *0226192-01-RIG-BER-001 rev00 Teknisk beregningrapport – Parametere*. O. Multiconsult.

Multiconsult. (2021a-b). *10226192-01-RIG-BER-001 rev00 Teknisk beregningrapport. Parametere* (Oslo: Multiconsult, Issue.

Multiconsult. (2021b). *10226192-01-RIG-BER-002 Teknisk beregningsrapport - Stabilitetsberegninger*. O. Multiconsult.

Rippa, S. (1999). An algorithm for selecting a good value for the parameter c in radial basis function interpolation. *Advances in Computational Mathematics*, *11*(2-3), 193-210. https://doi.org/Doi 10.1023/A:1018975909870

Rogstad, A. (2021). *Gjerdrum landslide: a study of the initial slide* (Department of Civil and Environmental Engineering, Norwegian University of Science and Technology

Issue.

Ryan, I., Ottesen, H. B., Nordal, S., Bruvoll, A., Hæreid, G. O., Solberg, I.,, & al., e. (2021). *Årsakene til kvikkleireskredet i Gjerdrum 2020*.

Toril Wiig, S.-A. S. o. E. D. H. (2020). *Sikkerhet mot kvikkleireskred*. N. v.-o. energidirektorat.

Tran, Q. A., Rogstad, A., Grimstad, G., Nordal, S. r., & Alene, G. H. (2022). Preliminary study of 3D large deformation modeling of the Gjerdrum 2020 sensitive clay landslide. the 8th Canadian Conference on Geotechnique and Natural HazardsAt: Quebec, Canada,

Tran, Q. A., & Solowski, W. (2019). Generalized Interpolation Material Point Method modelling of large deformation problems including strain-rate effects - Application to penetration and progressive failure problems. *Computers and Geotechnics*, *106*, 249-265. https://doi.org/10.1016/j.compgeo.2018.10.020

Virtanen, P., Gommers, R., Oliphant, T. E., Haberland, M., Reddy, T., Cournapeau, D., Burovski, E., Peterson, P., Weckesser, W., Bright, J., van der Walt, S. J., Brett, M., Wilson, J., Millman, K. J., Mayorov, N., Nelson, A. R. J., Jones, E., Kern, R., Larson, E., . . . Contributors, S. (2020). SciPy 1.0: fundamental algorithms for scientific computing in Python (vol 33, pg 219, 2020). *Nature Methods*, *17*(3), 352-352. https://doi.org/10.1038/s41592-020-0772-5

Zhang, X., Wang, L., Krabbenhoft, K., & Tinti, S. (2020). A case study and implication: particle finite element modelling of the 2010 Saint-Jude sensitive clay landslide. *Landslides*, *17*(5), 1117-1127. https://doi.org/10.1007/s10346-019-01330-4